Journal of Biomolecular NMR, **14:** 297–306, 1999.
KLUWER/ESCOM

Evidence for extensive anisotropic local motions in a small enzyme using a new method to determine NMR cross-correlated relaxation rates in the absence of resolved scalar coupling

Yuxi Pang[a], Lincong Wang[a], Maurizio Pellecchia[a], Alexander V. Kurochkin[a] & Erik R.P. Zuiderweg[a,b,c,*]

[a]*Biophysics Research Division,* [b]*Department of Biological Chemistry, and* [c]*Department of Chemistry, University of Michigan, 930 N. University Avenue, Ann Arbor, MI 48109-1055, U.S.A.*

Received 10 March 1999; Accepted 12 June 1999

Key words: anisotropy of local motions, Binase, ^{13}CO chemical shielding anisotropy, dipole-CSA cross-correlated relaxation, protein backbone dynamics

Abstract

Transverse ^{13}CO-^{1}HN (dipole-dipole)/^{13}CO (CSA) cross-correlated relaxation rates were measured for the ^{13}CO resonances of the protein ribonuclease Binase from *Bacillus intermedius* (12.3 kDa). This was carried out with a novel E.COSY-type triple-resonance experiment, which allows the measurement of cross-correlated transverse relaxation rate from multiplet effects in the absence of resolved scalar coupling. The ^{13}CO-^{1}HN (dipole-dipole)/^{13}CO (CSA) cross-correlated relaxation rates were determined with an average precision of $\pm 5\%$ and cover a range of values between -1.5 and $+0.6$ Hz. The average (-0.44 Hz) is to be compared with the computed value of -0.83 Hz for this interaction. Mechanisms that potentially can cause the average to be smaller than the theoretical value and the unexpected large spread in observed values are discussed. It is suggested that large contributions to the variations are due to large amplitude local anisotropic motions.

Introduction

NMR relaxation studies can provide detailed insight into internal motions of proteins (for a review see, e.g., Daragan and Mayo, 1997). In the past decade, ^{15}N spin relaxation methods have been developed which utilize the ^{15}N-^{1}HN bond vector as a probe to sense protein backbone dynamics (Kay et al., 1989a; Clore et al., 1990; Peng and Wagner, 1994). However, a single probe vector cannot properly characterize the anisotropy of local motions. For example, a local motion which can be described as a rotation around an axis parallel to the ^{15}N-^{1}HN bond vector does not modulate the ^{15}N-^{1}HN dipolar interaction, does therefore not cause ^{15}N spin relaxation and hence is not detected (see, e.g., Fischer et al., 1998a,b). It is thus appropriate to employ multiple relaxation probes to monitor local motions from different directions, and protein back bone relaxation studies have therefore been extended to the ^{13}CO nucleus (Cordier et al., 1996; Zeng et al., 1996; Dayie et al., 1997; Engelke and Rüterjans, 1997; Fischer et al., 1997, 1998a,b). While this spin is mainly relaxed by chemical shielding anisotropy (CSA) and dipole-dipole interaction with ^{13}Cα, several other relaxation mechanisms contribute significantly, making it difficult to interpret ^{13}CO relaxation data in a quantitative fashion.

By measuring cross correlation (interference) of relaxation one has the unique opportunity of selectively measuring a well-defined subset of relaxation mechanisms. Cross-correlated relaxation properties can provide rich dynamical and structural information about the protein backbone (Werbelow and Grant, 1977; Vold and Vold, 1978; Goldman, 1984; Dalvit and Bodenhausen, 1990; Tjandra et al., 1996; Daragan and Mayo, 1997; Fischer et al., 1997; Tessari

*To whom correspondence should be addressed. E-mail: zuiderwe@umich.edu.

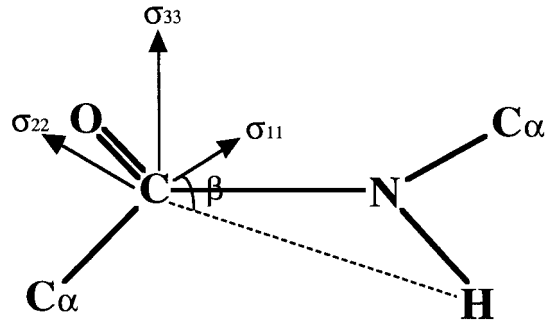

Figure 1. Schematic representation of the orientations of the ^{13}CO chemical shielding tensor within a peptide plane in which $\sigma_{33}(\sigma_{33} > \sigma_{22} > \sigma_{11})$ is the most shielded principal component ($\sigma_{11}-\sigma_{33} = -154$ ppm, $\sigma_{22}-\sigma_{33} = -88$ ppm (Teng et al., 1992). The dashed line indicates the dipolar interaction ^{13}CO–^{1}HN, which is at an angle $\beta = -62°$ with the ^{13}CO CSA principal axis σ_{11}.

et al., 1997; Reif et al., 1997). Consider, for example, the transverse cross-correlated relaxation rate $\Gamma_{I,IS}^{CSA/DD}$ for a rhombic CSA tensor of spin I with the dipolar interaction between spins I and S, which is determined by (Goldman, 1984; Daragan and Mayo, 1997; Fischer et al., 1997):

$$\begin{aligned}\Gamma_{I,IS}^{CSA/DD} = {} & K\{(\sigma_{11}-\sigma_{33})(4j^{11,IS}(O) \\ & +3J^{11,IS}(\omega_I)) \\ & +(\sigma_{22}-\sigma_{33})(4J^{22,IS}(O) \\ & +3J^{22,IS}(\omega_I))\}\end{aligned} \quad (1)$$

where

$$K = \frac{1}{6}\left(\frac{\mu_0}{4\pi}\right)\frac{\hbar\omega_I\gamma_I\gamma_s}{r_{IS}^3}$$

and

$$j^{ii,IS}(\omega) = \frac{2}{5}\left\{\begin{array}{l}\dfrac{S_{ii,IS}\tau_c}{1+(\omega\tau_c)^2}+ \\ \dfrac{(P_2(\cos\,\theta_{ii,IS})-S_{ii,IS})\tau}{1+(\omega\tau)^2}\end{array}\right\} \quad (2)$$

with

$$P_2(\cos\,\theta_{ii,IS}) = \frac{1}{2}(3\,\cos^2\,\theta_{ii,IS}-1)$$

The symbols have their usual meaning: the permeability of the free space is denoted by μ_0, $\hbar$ is Planck's constant divided by 2π, ω_I is the angular resonance frequency of spin I, γ_S and γ_I are the gyromagnetic ratios for spins S and I, respectively, and r_{IS} is the distance between the two nuclei. τ_c is the rotational correlation time; $\tau^{-1} = \tau_c^{-1} + \tau_e^{-1}$, where τ_e is the local correlation time. The principal values of the CSA tensor of spin I are indicated by σ_{ii}, where $i = 1, 2, 3$. The angle between the principal axis ii of the CSA tensor of I and the IS dipolar interaction vector is denoted as $\theta_{ii,IS}$. The quantity $S_{ii,IS}$ is the product of the (non-squared) order parameters of the vectors ii and IS, i.e., the 'cross-correlation order parameter' ($|P_2(\cos\,\theta_{ii,IS})| \geq |S_{ii,IS}| \geq 0$) which is sensitive to local motions on the time scale τ_e. The equations show that measurement of dipole-CSA cross-correlated transverse relaxation rates gives access to the geometric parameters $\theta_{ii,IS}$, the CSA tensor elements σ_{ii} and local motions described by $S_{ii,IS}$ and τ_e.

There are two methods available to measure dipole-CSA cross-correlated relaxation rate constants. The first one, in principle suitable for determining both transverse and longitudinal cross-correlation rates, is an incoherent magnetization transfer method in which one (two) spin term(s) can be induced to evolve partially into two (one) spin terms by cross-correlated relaxation, that is, $I_i \longleftrightarrow 2I_iS_z$(i=x, y, z). Using this method, ^{15}N-^{1}HN (DD)/^{15}N (CSA) (Tjandra et al., 1996), ^{15}N-^{1}HN (DD)/^{1}HN (CSA) (Tessari et al., 1997a,b), ^{13}Cα-^{1}Hα(DD)/^{13}Cα(CSA) (Tjandra and Bax, 1997) and ^{15}N-^{13}CO (DD)/^{13}CO (CSA) (Ghose et al., 1998) transverse cross-correlation rates have been determined and used to evaluate the anisotropy of the CSA tensors, assuming absence of local motion. Recently, applications aiming to make longitudinal cross-correlation rate measurements feasible have appeared as well (Felli et al., 1998; Kroenke et al., 1998). The second method is applicable only to the determination of cross-correlated transverse relaxation rates, and measures multiplet linewidth differentials. These experiments are commonly carried out using constant-time methods, where the different transverse relaxation rates of the multiplet components are manifested by differences of their intensities. Calculation of the intensity ratios of multiplet components then gives the desired cross-correlated relaxation rate constants. For example, ^{13}CO-^{13}Cα(DD)/^{13}CO (CSA) transverse cross-correlated relaxation rates have been determined by measuring ^{13}CO line intensity differentials for the $^{1}J_{CO-C\alpha}$ doublet and were interpreted in terms of anisotropy of local motions (Fischer et al., 1997). Based on the same principle, different cross-correlated transverse relaxation rates among ^{15}N, ^{13}CO and ^{1}HN spins within the peptide planes have been investigated in ZQ/DQ HNCO(H) experiments and analyzed in terms of Gaussian axial fluctuations describing local

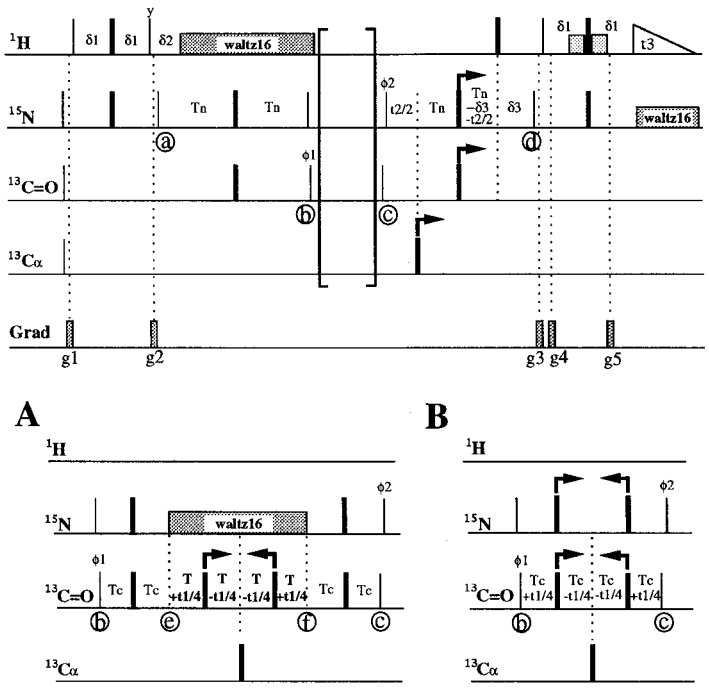

Figure 2. Pulse sequence for the determination of ^{13}CO-^{1}HN (DD)/^{13}CO (CSA) cross-correlated transverse relaxation rates. Panel A shows the sequence for the basic experiment; panel B is the reference experiment. Narrow and wide bars denote 90° and 180° hard pulses, respectively. Pulse phases are along the x-axis unless indicated otherwise. 90° and 180° square soft pulses with duration 65 μs and 130 μs were used for both ^{13}CO and ^{13}Cα. The half-sine-shaped field gradient pulses of 1 ms duration had strengths at the center g1 = 30 G/cm, g2 = 18 G/cm, g3 = 18 G/cm, g4 = 24 G/cm and g5 = 24 G/cm. Constant time periods 4T (4Tc in panel B) and 2Tn were used as ^{13}CO and ^{15}N chemical shift evolution periods, respectively. The delays were tuned for the relaxation properties of Binase (12.3 kDa, $\tau_c = 6.0 \pm 0.5$ ns at 303 K) as follows: δ1 = 2.6 ms, δ2 = 5.5 ms, Tn = 14 ms, Tc = 14 ms and T = 20 ms. Phase cycling was: φ1 = x,−x; φ2 =x, x, −x, −x; receiver = +, −, −, +. States-TPPI phase shifting was applied to φ1 and φ2 to achieve quadrature detection in the t_1 and t_2 time domains respectively, with spectral widths of 1724 Hz (F_1, ^{15}N), 1515 Hz (F_2, ^{13}CO), 8333 Hz (F_3, ^{1}HN). ^{15}N and ^{1}HN decoupling was carried out with 1.25 and 4.5 kHz r.f. fields, respectively. The WATERGATE scheme was used to saturate the solvent resonance (Piotto et al., 1992). The recycle delay was about 1 s. The 3D data were recorded with 36∗50∗1024 complex points (t_1∗t_2∗t_3). Experiment A was recorded with 16 scans per increment, for a measuring time of 37 h. Experiment B was recorded with 4 scans per increment, for a measuring time of 8 h. Both experiments were recorded in duplicate.

peptide plane anisotropic motions (Brutscher et al., 1998).

Measurement of cross-correlated relaxation rates in both methods depends on the existence of a direct scalar coupling between the nuclei involved in coherence and a dipolar-coupled spin. It is thus impossible to use these when the direct scalar coupling is very small, which excludes several interesting cross-correlation rates in the peptide plane from being measured. We propose here to separate unresolved multiplet components using an E.COSY strategy, commonly used to measure small scalar couplings (Griesinger et al., 1985, 1986, 1987; Montelione, 1992; Weisemann et al., 1994). In principle, this method allows accurate determinations of cross-correlated transverse relaxation rates even when the direct scalar coupling is vanishingly small. In the following we describe an experiment, modified from the well-known 3D HNCO pulse sequence (Kay et al., 1989b), to measure the cross-correlated transverse relaxation ^{13}CO-^{1}HN (DD)/^{13}CO(CSA) (see Figure 1). This cross-correlated relaxation is of interest because it is expected to be very sensitive to variations in the parameters of Equations 1 and 2, and because it is present as an unresolved component in a recently published experiment (Brutscher et al., 1998). The cross-correlated transverse relaxation rate cannot be obtained in direct ways since the direct scalar coupling between ^{13}CO and ^{1}HN is too small to allow the multiplet to be resolved ($^{2}J_{CO-NH} \approx$ 2.4–5.5 Hz) (Bystrov, 1976).

Experimental development

Figure 2A shows the pulse sequence for measuring the cross-correlated relaxation ^{13}CO-^{1}HN (DD)/^{13}CO (CSA), which is analogous to the 3D HNCO scheme in terms of magnetization transfer steps (Kay et al., 1989b; Grzesiek and Bax, 1990). Magnetization is transferred from ^{1}HN to ^{15}N at point **a** and further to the ^{13}CO spin, creating antiphase coherence $2C'_yN_z$ at point **b** by using two successive INEPT transfer steps. In order to isolate the interaction between ^{13}CO and ^{1}HN (see below) an additional Rev-INEPT step was used to refocus C'_yN_z into in-phase term C'_x at point **e**. ^{15}N composite pulse decoupling was applied while ^{13}Cα was decoupled by a 180 degree selective square pulse in the middle of the constant time period (4T) between points **e** and **f**, during which the ^{13}CO spin is scalar and dipolar coupled with ^{1}HN. The doublet components relax with different rates due to ^{13}CO-^{1}HN (DD)/^{13}CO (CSA) transverse cross correlation, denoted by $\Gamma_{C'}$, which we wish to measure. If these two doublet components would be well resolved, the cross-correlated transverse relaxation rate $\Gamma_{C'}$ could be easily obtained by calculating the intensity ratio of the two lines (Fischer et al., 1997). As indicated above, that is not the case.

To provide for the necessary resolution in an indirect way, the two ^{1}HN states are subsequently separated by the 90 Hz scalar coupling with the ^{15}N spin during a ^{15}N constant time chemical shift evolution period between points **c** and **d**. This period was also used to transfer the coherence back to ^{1}HN for detection. Thus, an E.COSY- type cross peak arrangement is generated in the ^{13}CO-^{15}N plane of the 3D experiment where the ^{13}CO doublets unresolved along the ^{13}CO dimension become completely separated along the ^{15}N dimension due to the large coupling $^{1}J_{N-HN}$ (see Figure 3). As the scalar coupling $^{1}J_{N-HN}$ is active between points **c** and **d**, so is the ^{1}HN-^{15}N dipolar coupling. Thus, the two unbalanced ^{13}CO doublet intensities were further changed by ^{15}N-^{1}HN (DD)/^{15}N (CSA) transverse cross correlation, denoted Γ_N. In addition, complex three-spin cross-correlation effects, denoted as $\Gamma_{C'NH}$, between ^{1}HN, ^{13}CO and ^{15}N occur between **b** and **e** and between **f** and **c**. After ^{15}N constant time chemical shift evolution at point **d**, the intensities $I^{\alpha}(d)$ and $I^{\beta}(d)$ for the multiplet components associated with ^{1}HN in $|\alpha>$ or $|\beta>$ state are (Kumar and Madhu, 1996):

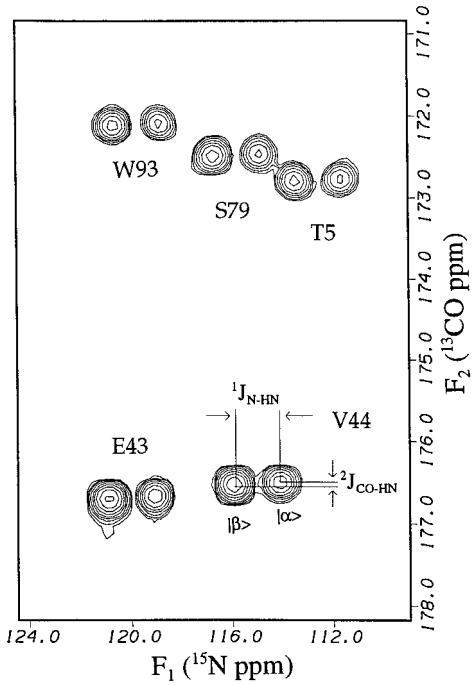

Figure 3. A representative ^{15}N-^{13}CO plane from the reference 3D spectrum, using the sequence of Figure 2B, which shows the E.COSY-type doublet arrangements. The scalar couplings are labeled along with the assignments. This spectrum was acquired at 303 K using a Bruker AMX-500 spectrometer equipped with a Nalorac 8 mm triple-resonance field gradient probe. The sample used was uniformly ^{15}N/^{13}C labeled Binase (12.3 kDa) at ~1.5 mM concentration in a Shigemi tube (90:10 H_2O:D_2O, pH 7).

$$I^{\alpha}(d) = I^{\alpha}(b)\exp -[4Tc(R_{C'NH} + \Gamma_{C'NH}) + 4T(R_C + \Gamma_C) + 2Tn(R_N + \Gamma_N)] \quad (3)$$

$$I^{\beta}(d) = I^{\beta}(b)\exp -[4Tc(R_{C'NH} - \Gamma_{C'NH}) + 4T(R_C - \Gamma_C) + 2Tn(R_N - \Gamma_N)] \quad (4)$$

where $I^{\alpha}(b)$ and $I^{\beta}(b)$ are the intensities of these multiplet components at time point **b.** $R_{C'}$ and R_N are ^{13}CO and ^{15}N transverse relaxation rates, respectively, including inhomogeneous broadening and chemical exchange effects. $R_{C'NH}$ is a net transverse relaxation rate including different interactions among ^{13}CO, ^{15}N and ^{1}HN spins during the rev-INEPT period between points **b** and **e** and between points **f** and **c**. The equations assume that the spontaneous proton flip rate is small as compared to the scalar coupling (see below). The sum of cross correlations, with different weights depending on the constant time periods (*T*, *Tn* and *Tc*) during which they are active, can be easily obtained by calculating the logarithmic intensity ratio *P* of the two

multiplet components at time point **d**, which is proportional to the intensities of these multiplet components in the final 3D spectrum:

$$P = \ln[I^{\beta}(d)/I^{\alpha}(d)] = 8T * \Gamma_{C'} + 4Tn * \Gamma_N + 8Tc * \Gamma_{C'NH} \quad (5)$$

The desired rate $\Gamma_{C'}$ can be obtained if a reference experiment is recorded with a different delay time *T*. We used a reference experiment with *T* equal to zero in which the ^{13}CO chemical shift labeling was carried out in the Rev-INEPT period between points **b** and **c** as shown in the sequence of Figure 2B. The logarithmic ratio *Q* of the doublet intensities from this reference experiment can be written as:

$$Q = \ln[I^{\beta}_{\mathrm{ref}}(d)/I^{\alpha}_{\mathrm{ref}}(d)] = 4Tn * \Gamma_N + 8Tc * \Gamma_{C'NH} \quad (6)$$

By substitution of Equation 6 into Equation 5, one obtains:

$$\Gamma_{C'} = (P - Q)/8T \quad (7)$$

Results and discussion

The experiment of Figure 2 was carried out with a 1.5 mM solution of uniformly ^{15}N/^{13}C labeled Binase (12.3 kDa), pH 7.0 in 90% H_2O. Three-dimensional NMR spectra were acquired at 303 K using a Bruker AMX-500 spectrometer equipped with a Nalorac 8 mm triple-resonance Z-gradient probe. Two experiments according to Figure 2A were recorded as well as two experiments according to Figure 2B. The total experimental time for the four experiments combined was 88 h. Figure 3 shows a representative ^{15}N-^{13}CO plane taken from the 3D spectrum, in which doublet components with different intensities were completely resolved. Not only dipolar information can be determined from this 2D spectrum; scalar coupling constants and the relative sign of $^{1}J_{N-HN}$ and $^{2}J_{CO-HN}$ can also be obtained. Figure 4A shows slices taken through duplicate spectra recorded with the sequence of Figure 2A, while Figure 4B shows similar data for the data obtained for the sequence of Figure 2B. After the reproducibility was found to be excellent, the duplicate data sets were added to yield two final 3D data sets. Figure 4C shows an overlay of these two spectra, that is, the difference seen is caused by the cross-correlated transverse relaxation ^{13}CO-^{1}HN (DD)/^{13}CO (CSA) that we desire to measure according to Equation 7. The peak intensities of the doublet components in these two spectra were obtained using the program NMRPipe (Delaglio et al., 1995). Individual peak intensities typically could be obtained with a precision of $\pm$0.5% as reported by the peak-fitting routine in the program. To obtain the error bars for the cross-correlated relaxation rates reported in Figure 5, the absolute errors in the peak intensities were propagated by repeated use of the following equation of statistics (Barford, 1967):

$$\Delta F(x_1, x_2, \ldots, x_n) = \sqrt{\sum_{i=1}^{n} \left(\frac{\partial F}{\partial x_i} \Delta x_i \right)^2} \quad (8)$$

On average, the absolute error bars reported in Figure 5 correspond to a relative error of $\pm$15%.

Figure 5 shows the obtained ^{13}CO-^{1}HN (DD)/^{13}CO (CSA) cross-correlated transverse relaxation rates for Binase. The average value is -0.44 Hz, with an rms variation of $\pm$0.45 Hz over all residues, and with a total range between -1.5 and $+0.6$ Hz. The high precision of the individual data points as indicated by the error bars ($\pm$ one standard deviation or 70% confidence limits) ensures that the variations observed are statistically significant. The variations do not correlate with the secondary structure of the protein (Pavlovsky et al., 1983; Kurochkin et al., 1991) as seen from Figure 5.

Recently, Ernst and co-workers reported (Brutscher et al., 1998) the measurement of the transverse remote cross-correlated relaxation ^{15}N-^{1}HN (DD)/^{13}CO(CSA) from differences in ^{1}HN multiplet intensities in double and zero quantum ^{15}N-^{13}CO coherence. Their method gives also access to the sum of the cross-correlated relaxation rates ^{13}CO-^{1}HN (DD)/^{13}CO(CSA) and ^{15}N-^{1}HN (DD)/^{15}N (CSA), which cannot be separated in their experiment. Our approach measures selectively the direct ^{13}CO-^{1}HN (DD)/^{13}CO(CSA) cross-correlated transverse relaxation rate, and its results can potentially be used in conjunction with the above methods.

Our new E.COSY cross-correlated transverse relaxation experiment paves the way for obtaining cross-correlated transverse relaxation rates for any pair of spins I and S, regardless of the magnitude of their direct scalar coupling, provided that a convenient coherence transfer pathway between them can be designed. This may lead to the development of many more experiments along the lines of the many E.COSY experiments in existence for measuring small scalar

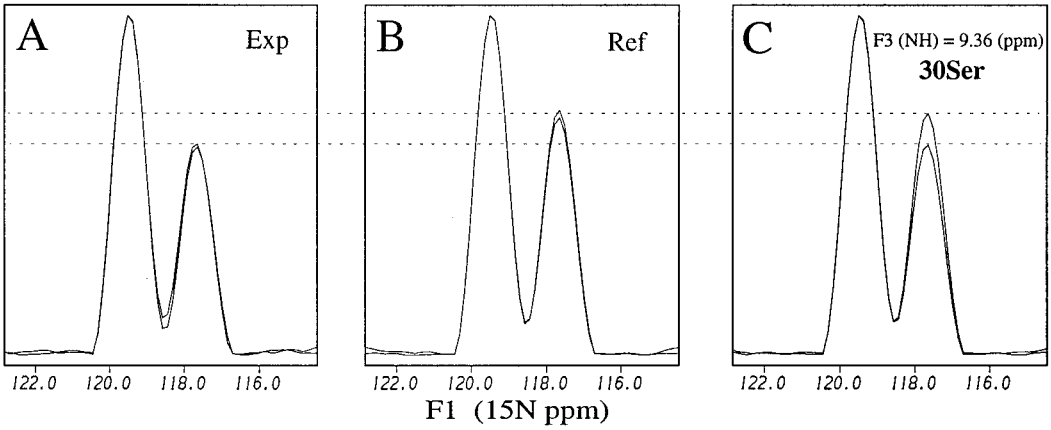

Figure 4. One-dimensional cross-sections through the 3D HNCO resonance of Ser30 along the ^{15}N dimension taken from 3D→ 2D projections on the ^{15}N-^{1}HN plane. The observed splitting corresponds to $^{1}J_{N-HN}$; the intensity differences are caused by transverse cross-correlation effects. Panel A illustrates the superposition and reproducibility of cross-sections taken from two duplicate experiments according to the sequence of Figure 2A. Panel B shows the superposition and reproducibility of cross-sections taken from two duplicate experiments according to the reference sequence of Figure 2B. Panel C shows a superposition of two cross-sections, one taken from the sum of the two duplicate experiments of panel A, and one taken from the sum of the two duplicate experiments of panel B. The difference in the doublet intensities in panel C, indicated by the dashed horizontal lines, is caused by the ^{13}CO-^{1}HN (DD)/^{13}CO (CSA) transverse cross correlation rate we wish to measure. This figure serves for purposes of illustration only; actual peak intensities were measured from the unprojected 3D spectra at the exact locations of the maximum intensities of the E.COSY-shifted multiplet components as shown in Figure 3. Experimental error estimation and propagation was carried out from measured signal/noise ratios in spectra such as Figure 3 using the program NMRPipe (see text).

couplings. However, one must bear in mind that, in *complete* absence of direct scalar coupling, significant attenuation of magnetization of the type $2I^{+}S_{z}$ can occur by S spin T_1 relaxation (see below).

The experiment of Figure 2 is designed to measure the process $C^{+} \rightarrow 2C^{+}H_{z}$ by CSA-dipolar cross correlation. One may be tempted to perform the same experiment while omitting the refocusing delay T_C to obtain better sensitivity. This would lead to the presence of $2C^{+}N_{z}$ coherence at the beginning of *T*, which will indeed transform to $4C^{+}N_{z}H_{z}$ magnetization under the influence of ^{13}CO-^{1}HN (DD)/^{13}CO (CSA) transverse cross correlation. A severe complication is that this same transformation also takes place under the influence of ^{15}N-^{1}HN (DD)/^{15}N (CSA) longitudinal cross-correlation. As the latter term is actually the larger one, the anti-phase experiment is uninterpretable. These complicated processes do of course also occur in the time periods between **b** and **e** and between **f** and **c** in the pulse sequence and are denoted by the complex rate $\Gamma_{C'NH}$. As shown above, they can be accounted for by obtaining a reference experiment.

The transverse dipole-dipole/CSA cross correlation I-S (DD)/S (CSA) between two spins 1/2 S and I has been written in terms of structural and dynamical parameters in Equations 1 and 2. In first approximation, the ^{13}CO-^{1}HN (DD) / ^{13}CO (CSA) cross-correlated transverse relaxation rates are expected to be constant over the protein sequence since there are no parameters in these equations that are explicitly dependent on protein conformation. Solid-state NMR studies (Teng et al., 1992) show that the CSA tensor principal axes σ_{11} and σ_{22}($\sigma_{11} < \sigma_{22} < \sigma_{33}$) lie on the peptide plane with an angle of $-62°$(β) and 206° to the ^{13}CO-^{1}HN vector, respectively, as shown in Figure 1; the anisotropy component of σ_{11}-σ_{33} is -154 ppm and that of σ_{22}-σ_{33} is -88 ppm. The internuclear distance between ^{13}CO and ^{1}HN is $r_{C'NH}$=2.06 Å according to standard trans-peptide geometry. With an average overall rotational correlation time τ_c of 6.0 ± 0.5 ns as obtained from ^{15}N relaxation measurements, one calculates for $\Gamma_{C'}$ a value of -0.83 Hz, in absence of local motion, in good agreement with the maximum values shown in Figure 5, but about twice as large as the observed average rate of -0.44 Hz.

The key question is what causes the observed average quenching and variations in the cross-correlated transverse relaxation. We consider the following potential sources of systematic errors and of inherent variabilities. The measured rates may systematically be reduced by 10–20% resulting from the incomplete inversion of the proton spins during the ^{15}N evolution. While substantial, this potential systematic error cannot account for the observed average quenching of the

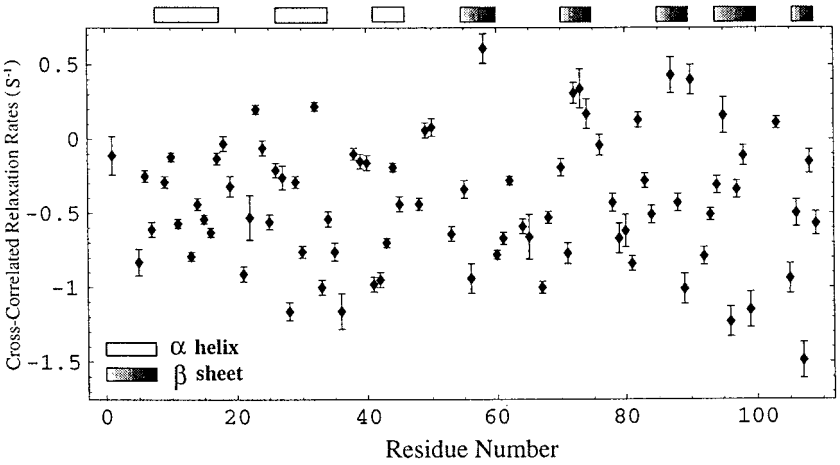

Figure 5. Experimental ^{13}CO-^{1}HN (DD)/^{13}CO (CSA) cross-correlated transverse relaxation rates for the ribonuclease Binase. Experimental uncertainties, propagated from errors as measured from signal/noise ratios are indicated by error bars (see text). The locations of elements of regular secondary structure for this protein are indicated at the top of the figure.

cross-correlated relaxation rates. Another systematic reduction of the measured rates can result from rapid relaxation of the $2C^{+}H_{z}$ coherence by ^{1}HN T_1 relaxation. This mechanism is normally only significant for longitudinal cross correlation (Kay et al., 1992; Felli et al., 1998) but needs to be considered for cross-correlated transverse relaxation rates with very small scalar coupling. The process is described by the equations (Goldman, 1984; Cavanaugh et al.,1996; Fischer et al., 1997):

$$\frac{dC^{+}H_{\alpha}}{dt} = -\left(R_{av} + R_{flip} + i\frac{^{2}J_{CO-HN}}{2} + \Gamma_{C'}\right) C^{+}H_{\alpha} - (R_{diff} - R_{flip})C^{+}H_{\beta} \quad (9)$$

$$\frac{dC^{+}H_{\beta}}{dt} = -\left(R_{av} + R_{flip} - i\frac{^{2}J_{CO-HN}}{2} - \Gamma_{C}\right) C^{+}H_{\beta} - (R_{diff} - R_{flip})C^{+}H_{\alpha} \quad (10)$$

where $C^{+}H_{\alpha}$ and $C^{+}H_{\beta}$ are the density matrix components describing the two transitions of the CO spin during the period between **e** and **f** in Figure 2 and where $^{2}J_{CO-HN}$ is the relevant scalar coupling. R_{av} and R_{diff} are the average and half difference of in-phase and antiphase relaxation rates, respectively; R_{flip} is one-half the spontaneous proton flip rate that interconverts the two transitions and in principle can average out their relaxation differences. Numerical integration of these equations using the values of 4 Hz for $^{2}J_{CO-HN}$, 3 s^{-1} for R_{av}, 1 s^{-1} for R_{diff}, -1 s^{-1} for $\Gamma_{C'}$, and 2 s^{-1} for R_{flip} demonstrated, however, that even such a fast flip rate reduces the apparent measured cross-correlated transverse relaxation rate by only 4%. This potential source of systematic error can thus be neglected for the present case.

Potentially more interesting inherent molecular mechanisms that may cause variabilities of the observed fluctuations and quenching of cross-correlated transverse relaxation rates include (i) overall anisotropic tumbling; (ii) variations in CSA tensor principal axes directions; (iii) static variations in peptide plane geometry; (iv) variations in CSA tensor principal values; and (v) anisotropic local motion of the peptide plane. Mechanism (i): with molecular size axis aspect ratios of 1.8: 1.2: 1, as measured from the Binase X-ray crystal structure coordinates (Pavlovsky et al., 1983; G. Dodson, personal communication), we compute, according to theory (Woessner, 1962), effective J(0) values that vary between 4.2 and 5.1 ns depending on the orientation of the relaxation vector with respect to the diffusion tensor. This would lead to maximally $\pm$10% variation in auto-relaxation rates for the different orientations, and less for cross-correlated transverse relaxation rates between vectors that are not collinear. Mechanism (ii): the internuclear vector ^{13}CO-NH is at an angle ($\beta = -64°$) with respect to the ^{13}CO CSA tensor principal axis σ_{11}. Calculations based on the full Equations 1 and 2 show that the effect of variations of β within reasonable limits, based on solid-state NMR reports documenting variations in the tensor principal axes (see, e.g., Fischer et al., 1997), can cause at most $\pm$15% variation in cross-correlated transverse relaxation rate (Figure 6a). Mechanism (iii): investigation of the coordinates of a

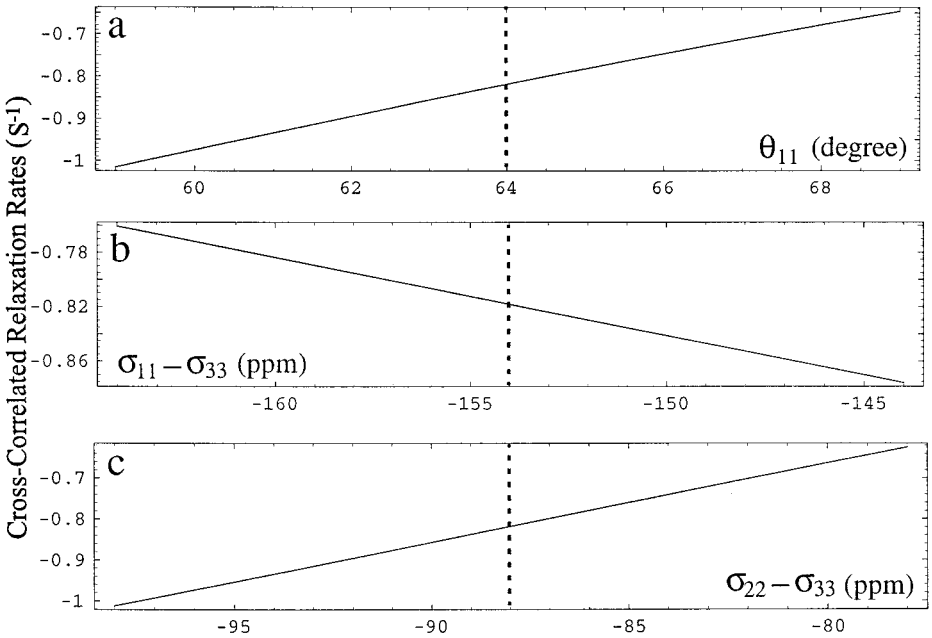

Figure 6. Computed dependency of ^{13}CO-^{1}HN (DD)/^{13}CO (CSA) cross-correlated transverse relaxation rates on the angle θ_{11} (β) between the vectors ^{13}CO-^{1}HN and σ_{11} (top), the value for the ^{13}CO CSA element σ_{11}-σ_{33} (middle); and the value for the ^{13}CO CSA element σ_{22}-σ_{33} (bottom). No local motions were included in these calculations. The literature values of the CSA parameters (Teng et al., 1992) are indicated by the dashed line. The computations and graphs were made with the program Mathematica 3.0.

0.83 Å resolution X-ray structure of the protein Crambin (Teeter et al., 1993) indicates that the peptide plane dihedral angle ω in proteins may vary between -173 and $+173°$ for non-proline residues. This variation will give rise to (and may be the cause of?) similar variances in the angle β as discussed above, and will hence give rise to similar variations in cross-correlation rates. Mechanism (iv): literature data, from solid state NMR (De Dios et al., 1994) and from ab initio calculations (Sitkoff and Case, 1998), indicates that significant variations for the ^{13}CO CSA tensor anisotropy's σ_{22}-σ_{33} and σ_{11}-σ_{33} may be attributed to variations in hydrogen bonding and can amount to $\pm$10 ppm. Calculations based on the full Equations 1 and 2 show that these relatively large differences give rise to at most $\pm$15% variation in cross-correlation rates (Figure 6b and c). Mechanism (v): Equations 1 and 2 show that the net cross-correlated transverse relaxation rate is dependent on two order parameters: one ($S_{11-C'H}$) which is sensitive to local rotational motions around vectors not collinear with σ_{11} or the ^{13}CO-^{1}HN vectors, the other ($S_{22-C'H}$) which is sensitive to local rotational motions around vectors not collinear with σ_{22} or the ^{13}CO-^{1}HN vectors. Figure 7 shows computations of the effects of local motions around three different axes on the cross-correlated transverse relaxation rates, obtained from

$$S_{ii,C'H} = \frac{4\pi}{5} \sum_{m=-2}^{2} \langle Y_{2m}(\theta_{ii}, \varphi_{ii}) \rangle \langle Y^{*}_{2m}(\theta_{C'H}, \varphi_{CH}) \rangle \tag{11}$$

where

$$\langle Y_{2m}(\theta_{ii}, \varphi_{ii}) \rangle = \int_0^{2\pi} \int_0^{\pi} Y_{2m}(\theta_{ii}, \varphi_{ii}) P_{ii}(\theta_{ii}, \varphi_{ii}) \sin\theta \, d\theta \, d\varphi \tag{12}$$

$P_{ii}(\theta_{ii}, \varphi_{ii})$ is a probability descriptor of the local motion of the principal axis ii; similar definitions apply to the vector C′H (^{13}CO-^{1}HN). The probability was modeled (Fischer et al., 1997) as an equal distribution of rotational states of these vectors around the direction of the motions for the range indicated in Figure 7. The figure indicates those differences in extent and direction of anisotropic local motions that can account for significant differences in the cross-correlated transverse relaxation rate. This is caused by the circumstance that the terms $(\sigma_{11} - \sigma_{33})(4J^{11,IS}(0) + 3J^{11,IS}(\omega))$ and $(\sigma_{22} - \sigma_{33})(4J^{22,IS}(0) + 3J^{22,IS}(\omega))$ in Equation 1 are rather similar in magnitude and opposite in sign; hence different directions of local

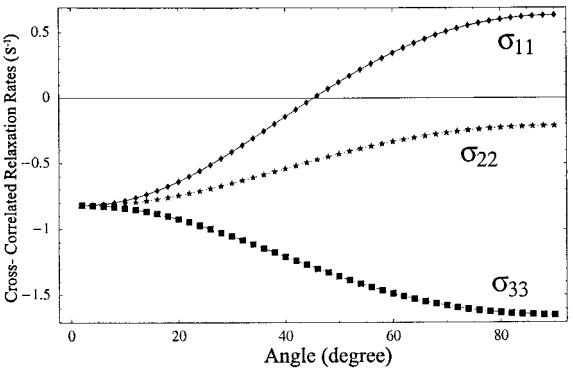

Figure 7. Computation of the variations of ^{13}CO-^{1}HN (DD)/^{13}CO (CSA) cross-correlated transverse relaxation rate with local anisotropic motions. The literature values of the CSA parameters (Teng et al., 1992) were assumed. The diamonds, stars and squares show the variation of the cross-correlated transverse relaxation rate upon rotational diffusion around vectors parallel to σ_{11}, σ_{22} and σ_{33}, respectively. A rotational diffusion angle of, e.g., 40° is defined as an even distribution over a range of ±40°. The computations and graphs were made with the program Mathematica 3.0, using Equations 1, 2, 11, and 12, modified from materials encoded by Dr. M.W.F. Fischer (Fischer et al., 1997).

motions that influence these two terms to only small extent affect the overall cross-correlated transverse relaxation rates considerably.

If we take all mechanisms as statistically independent, we compute, by adding the squares of the fluctuations and taking the square root, an average variation of ±28% in cross-correlated transverse relaxation rates for mechanisms (i)–(iv) combined, clearly far less than the experimental range shown in Figure 5 (experimental rms variation is ±0.45 Hz, or ±100% from the average value of −0.44 Hz). Even a computed range of ±55%, obtained when simply adding all mechanisms (i)–(iv), is insufficient to explain the observed spread and extremes.

Local anisotropic motion at the nano-picosecond time scale (mechanism (v)) can in principle account for the entire observed range of variations, if large local rotational motions, up to ±40°, are considered, as shown in Figures 5 and 7. Rotational fluctuations of ±30° around an axis parallel to σ_{11} will cause a reduction of the average cross-correlated transverse relaxation rate by a factor of two, as observed. Rotational fluctuations of ±60° around an axis parallel to σ_{33} will cause an unexpected *increase* in cross-correlated transverse relaxation rate to −1.5 Hz, as observed for a few residues.

Long-time molecular dynamics simulations of small proteins like BPTI (Brunne et al., 1995) and TGFα (Fadel et al., 1995) show that for the backbone dihedral angles Ψ and Φ at the 10 ps time scale, protein-averaged rms fluctuations of ±20° occur, while some residues show fluctuations of at least ±40°. The fluctuations are correlated for Ψ and Φ, and are caused by rotational mobility of the entire peptide plane along the C′-Cα(i–1) and N-Cα (i) bonds respectively (dubbed crankshaft motion, Fadel et al., 1995; Brutscher et al., 1998). This direction corresponds closely to the σ_{11} direction of the ^{13}CO CSA tensor (see Figure 1). Thus the crankshaft motions computed from the molecular dynamics trajectory for BPTI could have the correct time scale and direction to account for the observed average reduction in cross-correlated transverse relaxation rate in Binase. Molecular dynamics simulations for BPTI also indicate that for a few peptide planes inversions along the crankshaft axis can take place (fluctuations of ±90°) at a time scale of several hundred ps (Brunne et al., 1995). Such occurrences would explain the change in the sign of the cross-correlated transverse relaxation rate as is observed for several residues in Binase; however, most of these residues reside in β-strands (see Figure 5), which makes peptide plane inversion improbable. Very large variations in cross-correlated relaxation rates are observed for the C-terminal half of Binase. The directions of the major components of local motion appear to vary here from residue to residue. It is of interest to note that this area also contains the active site of the enzyme, for which extensive millisecond dynamics has been measured as well (to be published).

We conclude from these considerations, that our current studies provide further experimental evidence for the presence of extensive local dynamics which appears to vary greatly over the amino acid sequence. We have found no correlation between variations in the cross-correlated transverse relaxation rate and the protein secondary structure (see Figure 5). Therefore, there appears to be no clear correlation between the extent of the motions and the secondary structure either.

While a majority of the fluctuations in cross-correlated transverse relaxation rate over the amino acid sequence may be attributable to local motion, we certainly will not exclude variability in CSA tensor values and some of the other parameters discussed above. It is conceivable that large motions actually cause changes in the CSA tensor as hydrogen bonding is transiently disturbed, and that variations in CSA tensor axes correspond to variations in static or

dynamic peptide-plane geometry. Variation in mobility, CSA tensors and geometry, all of which affect the cross-correlated transverse relaxation according to Equations 1 and 2, can possibly be deconvoluted in a comprehensive investigation of the auto- and cross-correlated relaxation of many vectors of the peptide plane. Currently such a process is in progress in our laboratory.

Acknowledgements

We thank Drs. Anil Kumar and Mark Fischer for helpful discussions and Dr. Guy Dodson (University of York). This work was supported by grants MCB 9513355 and MCB 9814431 from the National Science Foundation.

References

Abragam, A. (1961) *The Principles of Nuclear Magnetism*, Clarendon Press, Oxford.
Barford, N.C. (1967) *Experimental Measurements: Precision, Error and Truth*, Wiley, New York, NY, pp. 36–37.
Boyd, J., Hommel, U. and Campbell, I.D. (1990) *Chem. Phys. Lett.*, **175**, 477–481.
Brunne, R.M., Berndt, K.D., Güntert, P., Wüthrich, K. and Van Gunsteren, W.F. (1995) *Proteins Struct. Funct. Genet.*, **23**, 49–62.
Brutscher, B., Skrynnikov, N.R., Bremi, T., Brüschweiler, R. and Ernst, R.R. (1998) *J. Magn. Reson.*, **130**, 346–351.
Bystrov, V.F. (1976) *Prog. NMR Spectrosc.*, **10**, 41–81.
Cavanaugh, J., Fairbrother, W.J., Palmer III, A.G. and Skelton, N.J. (1996) *Protein NMR Spectroscopy, Principles and Practice*, Academic Press, San Diego, CA, p. 279.
Clore, G.M., Szabo, A., Bax, A., Kay, L.E., Driscoll, P.C. and Gronenborn, A.M. (1990) *J. Am. Chem. Soc.*, **112**, 4989–4991.
Cordier, F., Brutscher, B. and Marion, D. (1996) *J . Biomol NMR*, **7**, 163–168.
Dalvit, C. and Bodenhausen, G. (1990) *Adv. Magn. Reson.*, **14**, 1–32.
Daragan, V.A. and Mayo, K.H. (1997) *Prog. NMR Spectrosc.*, **31**, 63–105.
Dayie, K.T. and Wagner, G. (1997) *J. Am. Chem. Soc.*, **119**, 7797–7806.
De Dios, A.C. and Oldfield, E. (1994) *J. Am. Chem. Soc.*, **116**, 11485–11488.
Delaglio, F., Grzesiek, S., Vuister, G.W., Zhu, G., Pfeifer, J. and Bax, A. (1995) *J. Biomol. NMR*, **6**, 277–293.
Engelke, J. and Rüterjans, H. (1997) *J. Biomol. NMR*, **9**, 63–78.
Fadel, A.R., Jin, D.Q., Montelione, G.T. and Levy, R.M. (1995) *J. Biomol. NMR*, **6**, 221–226.
Felli, I.C., Desvaux, H. and Bodenhausen, G. (1998) *J. Biomol. NMR*, **12**, 509–521.
Fischer, M.W.F., Zeng, L., Pang, Y., Hu, W., Majumdar, A. and Zuiderweg, E.R.P. (1997) *J. Am. Chem. Soc.*, **119**, 12629–12642.
Fischer, M.W.F., Zeng, L., Majumdar, A. and Zuiderweg, E.R.P. (1998a) *Proc. Natl. Acad. Sci. USA*, **95**, 8016–8019.
Fischer, M.W.F., Majumdar, A. and Zuiderweg, E.R.P. (1998b) *Prog. NMR. Spectrosc.*, **33**, 207–272.
Ghose, R., Huang, K. and Prestegard, H. (1998) *J. Magn. Reson.* **135**, 487–499.
Goldman, M. (1984) *J. Magn. Reson.*, **60**, 437–452.
Griesinger, C., Sørensen, O.W. and Ernst, R.R. (1985) *J. Am. Chem. Soc.*, **107**, 6394–6396.
Griesinger, C., Sørensen, O.W. and Ernst, R.R. (1986) *J. Chem. Phys.*, **85**, 6837–6852.
Griesinger, C., Sørensen, O.W. and Ernst, R.R. (1987) *J. Magn. Reson.*, **75**, 474–492.
Grzesiek, S. and Bax, A. (1990) *J. Magn. Reson.*, **96**, 432–440.
Hiyama, Y., Niu, C.H., Silverton, J.V., Bavoso, A. and Torchia, D.A. (1988) *J. Am. Chem. Soc.*, **110**, 2378–2383.
Kay, L.E., Torchia, D.A. and Bax, A. (1989a) *Biochemistry*, **28**, 8972–8979.
Kay, L.E., Ikura, M., Tschudin, R. and Bax, A. (1989b) *J. Magn. Reson.*, **89**, 496–514.
Kay, L.E., Nicholson, L.K., Delaglio, F., Bax, A. and Torchia, D.A. (1992) *J. Magn. Reson.*, **97**, 359–375.
Kroenke, C.D., Loria, J.P., Lee, L.K., Rance, M. and Palmer III, A.G. (1998) *J. Am. Chem. Soc.*, **120**, 7905–7915.
Kumar, A. and Madhu, P.K. (1996) *Conc. Magn. Reson.*, **8**, 139–160.
Kurochkin, A.V., Kirpichinov, M.P. and Rüterjans, H. (1991) *Doklady Biochemistry*, **321**, 282–286.
Lumsden, M.D., Wasylishen, R.E., Eichele, K., Schindler, M., Penner, G.H., Power, W.P. and Curtis, R.D. (1994) *J. Am. Chem. Soc.*, **116**, 1403–1413.
Montelione, G.T., Emerson, S.D. and Lyons, B.A. (1992) *Biopolymers*, **32**, 327–334.
Pavlovsky, A.G., Vagin, A.A., Vainstein, B.K., Chepurnova, M.K. and Karpeisky, M.Y. (1983) *FEBS Lett.*, **162**, 167–170.
Peng, J.W. and Wagner, G. (1994) *Nuclear Magnetic Resonance Probes of Molecular Dynamics*, (R. Tycko, Ed.), Kluwer, Dordrecht, pp. 373–454.
Piotto, M., Saudek, V. and Sklenar, V. (1992) *J. Biomol. NMR*, **2**, 661–665.
Reif, B., Henning, M. and Griesinger, C. (1997) *Science*, **276**, 1230–1233.
Sitkoff, D. and Case, D.A. (1998) *Prog. NMR Spectrosc.*, **32**, 165–190.
Teeter, M.M., Roe, S.M. and Heo, N.H. (1993) *J. Mol. Biol.*, **230**, 292–311.
Teng, Q., Iqbal, M. and Cross, T.A. (1992) *J. Am. Chem. Soc.*, **114**, 5312–5321.
Tessari, M., Mulder, F.A.A., Boelens, A. and Vuister, G.W. (1997a) *J. Magn. Reson.*, **127**, 128–133.
Tessari, M., Vis, H., Boelens, R., Kaptein, R. and Vuister, G.W. (1997b) *J. Am. Chem. Soc.*, **119**, 8985–8990.
Tjandra, N. and Bax, A. (1997) *J. Am. Chem. Soc.*, **119**, 9576–9577.
Tjandra, N., Szabo, A. and Bax, A. (1996) *J. Am. Chem. Soc.*, **118**, 6986–6991.
Vold, R.L. and Vold, R.R. (1978) *Adv. Magn. Reson.*, **12**, 79–133.
Weisemann, R., Rüterjans, H., Schwalbe, H., Schleucher, J., Bermel, W. and Griesinger, C. (1994) *J. Biomol. NMR*, **4**, 231–240.
Werbelow, L.G. and Grant, D.M. (1977) *Adv. Magn. Reson.*, **9**, 189–301.
Woessner, D.E. (1962) *J. Chem. Phys.*, **17**, 647–654.
Yang, D., Konrat, R. and Kay, L.E. (1998) *J. Am. Chem. Soc.*, **119**, 11938–11940.
Zeng, L., Fischer, M.W.F. and Zuiderweg, E.R.P. (1996) *J. Biomol. NMR*, **7**, 157–162.